Nanoscale Advances

PAPER

View Article Online
View Journal | View Issue

Cite this: *Nanoscale Adv.*, 2019, **1**, 696

Development of an efficient phenolic sensor based on facile Ag_2O/Sb_2O_3 nanoparticles for environmental safety†

Mohammed M. Rahman, *[ab] M. M. Alam [c] and Abdullah M. Asiri *[ab]

Received 12th June 2018
Accepted 24th October 2018

DOI: 10.1039/c8na00034d

rsc.li/nanoscale-advances

The facile hydrothermal method was used to prepare low-dimensional doped Ag_2O/Sb_2O_3 nanoparticles (NPs) at low temperature in alkaline medium. The calcined NPs were characterized in detail by FTIR, UV/vis, FESEM, XPS, EDS, and XRD. A thin layer of Ag_2O/Sb_2O_3 NPs was deposited onto a glassy carbon electrode (GCE) using Nafion (5% Nafion suspension in ethanol) conducting binder, which formed the working electrode of the selective 3-methoxyphenol electrochemical sensor probe. The proposed chemical sensor exhibits high sensitivity, long-term stability, and enhanced electrochemical responses towards 3-methoxyphenol. Response to 3-methoxyphenol is linear over the concentration range (LDR) of 0.09 nM to 0.09 mM. The analytical parameters of the sensor such as sensitivity, stability, response time, linearity, LDR, robustness, selectivity *etc.* were evaluated by an electrochemical approach. The sensor probe fabricated with Ag_2O/Sb_2O_3 NPs seems to be a promising candidate for effective and reliable electrochemical detection of hazardous and carcinogenic chemicals in the environment and health care fields in large scales.

Introduction

Phenol and its derivatives are responsible for the toxic contamination of water (ground and underground).[1] Due to the high environmental toxicity of phenol including humans, animals, plants, aquatic life and other living organisms,[2–4] phenolic compounds are considered as priority environmental pollutants by the United States Environmental Protection Agency (USEPA) and the European Commission. These pollutants generally come into the environment as waste effluent from various industries such as paper, dyes, detergent, resins, herbicides, pharmaceuticals, pesticides, explosives, plastics, coal mining and crude oil refining.[5,6] There are some traditional methods to detect phenolic compounds such as capillary electrophoresis, decent gas or liquid chromatography, spectrophotometry, fluorimetry, and mass spectrometry. However, these processes have the limitations of high cost, time consumption and complicated detection procedure.[7–10] In contrast, the electrochemical method (*I–V*) has great advantages such as low cost, simplicity of procedure, rapid and short response time, selectivity and good sensitivity.[11] Semi-conductive metal oxides with a wide band gap energy (eV) such as TiO_2, ZnO, SnO_2, Fe_2O_3, Ag_2O, and Sb_2O_3 have been exclusively investigated as sensing elements to assemble electrochemical sensors.[12–14] According to Rahman *et al.*, the 4-methoxyphenol sensor based on NiS_2/CNT nanocomposites exhibited good sensitivity (0.632 $\mu A\ \mu M^{-1}\ cm^{-2}$) with a low detection limit (30.0 pM).[15] Another report claimed that the phenolic sensor using 3D graphene micro-pillar showed a sensitivity of 3.9 nA $mM^{-1}\ cm^{-2}$ and a detection limit of 50.0 nM.[16] In the last decade, conducting polymer–carbon nanotubes (CNT) composited with various transition metal oxides achieved great attention as sensing material to fabricate chemical sensors. A 3-methoxyphenol chemical sensor based on poly (*o*-anisidine)/silverized multiwall carbon nanotube (POAS/Ag/MWCNT) nanocomposite exhibited higher sensitivity with a low detection limit.[17]

Since, 3-methoxyphenol is highly toxic and has serious risk of illness, an urgent initiative should be taken for its significant detection using a consistent and reliable technique. Herein, we report a 3-methoxyphenol chemical sensor based on Ag_2O/Sb_2O_3 nanoparticles by electrochemical method. A thin layer of synthesized NPs was deposited onto a GCE electrode with conducting binder to fabricate the working electrode of the 3-methoxyphenol chemical sensor. This working electrode detected the 3-methoxyphenol by a reliable electrochemical technique. It should be noted that the proposed chemical sensor is exceptional and newly developed based on Ag_2O/Sb_2O_3 NPs/binder/GCE. It is noted that the proposed chemical sensor

[a]*Chemistry Department, King Abdulaziz University, Faculty of Science, P.O. Box 80203, Jeddah 21589, Saudi Arabia. E-mail: mmrahman@kau.edu.sa; aasiri2@kau.edu.sa*
[b]*Center of Excellence for Advanced Materials Research, King Abdulaziz University, P.O. Box 80203, Jeddah 21589, Saudi Arabia*
[c]*Department of Chemical Engineering and Polymer Science, Shahjalal University of Science and Technology, Sylhet 3100, Bangladesh*

† Electronic supplementary information (ESI) available. See DOI: 10.1039/c8na00034d

is exceptional and newly developed sensor totally based on Ag_2O/Sb_2O_3 NPs/binder/GCE by electrochemical method.

Experimental sections

Materials and methods

Analytical grade chemicals such as ammonium hydroxide, Nafion (5% Nafion suspension in ethanol), acetone, 2-nitrophenol, 3-methoxyphenol, 4-aminophenol, 4-methoxyphenol, bisphenol A, ethanol, hydrazine, methanol, *p*-nitrophenol, monosodium phosphate and disodium phosphate were purchased from Sigma-Aldrich (USA). These were used as received. The maximum visible light absorption (λ_{max}) and the corresponding band gap energy (E_{bg}) of the synthesized Ag_2O/Sb_2O_3 NPs were investigated by UV/vis spectrophotometer and Thermo Scientific NICOLET iS50 FTIR spectrometer (Madison, WI, USA) was used to record FTIR spectrum. To quantify the binding energies (eV) of O, Ag and Sb, XPS was performed on the prepared Ag_2O/Sb_2O_3 NPs using K-α spectrometer (K-α1 1066, Germany). Elemental and morphological analyses of the Ag_2O/Sb_2O_3 NPs were examined by of FESEM (JEOL, JSM-7600F, Japan) analysis equipped with EDS. The phase crystallinity of the nanoparticles was explored by XRD patterns obtained at atmospheric condition. The current *vs.* potential technique was employed to detect 3-methoxyphenol at the required (0 to +1.5 V) range of applied electrical potential using a Keithley electrometer (6517A, USA). Ag_2O/Sb_2O_3 NPs were deposited on a GCE with the help of Nafion, a conducting binder, to construct the desired working electrode of the 3-methoxyphenol electrochemical sensor. The assembled chemical sensor was applied for successive detection of 3-methoxyphenol in phosphate buffer medium.

Preparation of Ag_2O/Sb_2O_3 NPs by hydrothermal process

Silver nitrate ($AgNO_3$), antimony tetrachloride ($SbCl_3$) and ammonium hydroxide (NH_4OH) were used as the reacting precursors to prepare Ag_2O/Sb_2O_3 NPs by hydrothermal method. The hydrothermal technique is a common system for the synthesis of doped nanomaterials with smaller grain size and phase formation. Following this technique, a conical flask (250.0 mL) was filled with 100 mL distilled water and measured amounts of $AgNO_3$ and $SbCl_3$ were dissolved in this conical flask with continuous magnetic stirring. To adjust the pH of the solution at 10.5, NH_4OH was added to the resultant solution and was kept inside a hydrothermal system at 150 °C for several hours. As stated in reactions (i) to (iv), $AgNO_3$ and $SbCl_3$ were hydrolyzed to form Ag^+ and Sb^{+3} and subsequently, the metal ions were co-precipitated in the form of metal hydroxides due to increase in pH. At pH 10.5, all the metal ions had precipitated quantitatively as $Ag(OH)\cdot Sb(OH)_3\cdot nH_2O$. The metal hydroxide formation is completely analogous with the reported articles.[18,19]

$$NH_4OH_{(s)} \rightarrow NH_{4(aq)}{}^{+} + OH_{(aq)}{}^{-} \quad \text{(i)}$$

$$AgNO_{3(s)} \rightarrow Ag_{(aq)}{}^{+} + NO_{(aq)}{}^{3-} \quad \text{(ii)}$$

$$SbCl_{3(s)} \rightarrow Sb_{(aq)}{}^{3+} + 3Cl_{(aq)}{}^{-} \quad \text{(iii)}$$

$$Sb_{(aq)}{}^{3+} + Ag_{(aq)}{}^{+} + 4OH_{(aq)}{}^{-} + nH_2O \leftrightarrows Sb(OH)_3\cdot Ag(OH)\cdot nH_2O_{(aq)} \quad \text{(iv)}$$

Finally, the resultant precipitate was separated from the reaction medium, washed with de-ionized water and acetone. After that, it was placed inside an oven at 110 °C overnight.

The produced metal hydroxides were calcined in a furnace (Barnstead Thermolyne, 6000 Furnace, USA) at 500 °C for around 6 hours. In the muffle furnace, the metal hydroxides were oxidized in the presence of atmospheric oxygen. According to the Ostwald-ripening method of nanoparticles growth mechanism, Ag_2O/Sb_2O_3 NPs nuclei are initiated by self- and mutual-aggregation and the nanocrystals are re-aggregated again at higher temperatures to form the Ag_2O/Sb_2O_3 nanocrystals. The molecular arrangement inside of the nanocrystals is based on the van der-Waals forces between each other's counterparts. The reaction in the muffle furnace is supposed to occur as below (v).

$$2Ag(OH)\cdot Sb(OH)_3 + O_2 \rightarrow Ag_2O\text{–}Sb_2O_{3(s)}\downarrow + 4H_2O_{(aq)} \quad \text{(v)}$$

The growth mechanism of the doped nanoparticles of Ag_2O/Sb_2O_3 is similar to the growth patterns reported previously.[20,21] The formation mechanism of Ag_2O/Sb_2O_3 NPs is presented in Scheme 1. This is the first time calcined Ag_2O/Sb_2O_3 NPs were applied to detect 3-methoxyphenol, and there is no report available regarding this.

Fabrication of GCE with Ag_2O/Sb_2O_3 NPs

A round rod-shaped glassy carbon nanotube (GCE) was used to fabricate the working electrode by coating Ag_2O/Sb_2O_3 NPs using the conducting binder 5% Nafion. 0.1 M phosphate buffer (PBS-solution) at pH 7.0 was prepared by mixing equimolar concentrations of 0.2 M Na_2HPO_4 and 0.2 M NaH_2PO_4 solutions in 100.0 mL de-ionized water at ambient conditions. The diameter of the tip of the working electrode is 1.0 mm. To fabricate the working electrode from GCE, a slurry of Ag_2O/Sb_2O_3 NPs was prepared in ethanol and used to coat on GCE at ambient conditions. For the improvement of the binding strength between the glassy carbon electrode and the Ag_2O/Sb_2O_3 NPs, a drop of Nafion (5% Nafion suspension in ethanol) was added on to the modified GCE. The slurry of NPs was prepared in ethanol and coated as thin uniform layer onto GCE. After drying, a drop of Nafion was added as chemical-glue to bind the material and improve the binding strength as well as electron transfer rate. Then, the electrode was placed inside an oven at 35.0 °C temperature until the conducting film was dried completely. An electrochemical cell was assembled with Ag_2O/Sb_2O_3 NPs/binder/GCE and Pt-wire (dia., 1.5 mm), where Ag_2O/Sb_2O_3 NPs/binders/GCE was acting as the working electrode and Pt-wire was the counter electrode. A range of 3-methoxyphenol solutions based on concentration (full concentration range: 0.9 mM to 0.09 nM) was prepared. The sensitivity of the modified working electrode based on Ag_2O/Sb_2O_3 NPs was measured from the slope of the calibration curve (the ratio of

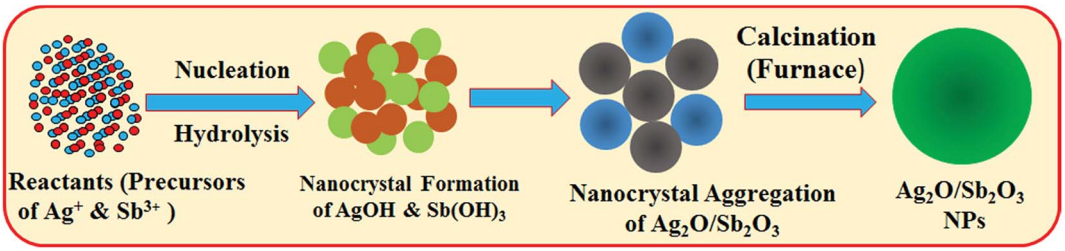

Scheme 1 Growth mechanism of Ag_2O/Sb_2O_3 NPs produced by the low temperature hydrothermal method.

current *versus* concentration). In the same way, the detection limit (DL) and the linear dynamic range (LDR) were calculated from the ratio of 3N/S (ratio of noise × 3 *vs.* sensitivity). The utilized electrometer is a simple two-electrode system and was supplied with a constant voltage for *I–V* measurement. The amount of 0.1 M PBS-solution was kept constant in the beaker as 10.0 mL throughout the chemical investigations.

Results and discussions

Choice of materials

Facile hydrothermally prepared Ag_2O/Sb_2O_3 NPs have employed a great deal of consideration due to their chemical, structural, physical, and optical properties in terms of large-active surface area, high-stability, high porosity, and permeability, which directly depend on their structural morphology. Ag_2O/Sb_2O_3 NPs were prepared by using the reactant precursors ($AgNO_3$ & $SbCl_3$) in a basic medium at low-temperature. They were synthesized by hydrothermal method using NH_4OH reducing agents at ambient conditions. This technique has several advantages including facile preparation, accurate control of reactant temperature, ease of handling, one-step reaction, and high-porosity. Optical, morphological, electrical, and chemical properties of the Ag_2O/Sb_2O_3 NPs are of huge significance from the scientific aspect compared to other undoped materials. Non-stoichiometry, mostly oxygen vacancies, makes it conducting in the nanomaterials. The formation energy of oxygen vacancies and metal interstitials in semiconductors is very low, and thus, these defects are formed easily resulting in experimentally elevated conductivity of the Ag_2O/Sb_2O_3 NPs compared to other undoped materials such as Ag_2O, Sb_2O_3, CuO, NiO, *etc.* Ag_2O/Sb_2O_3 NP materials have also attracted considerable interest owing to their potential applications in opto-electronics, electro-analytics, selective detection of bioassays, biological devices, hybrid-composites, electron-field emission sources for emission exhibits, biochemical detection, and surface-enhanced Raman properties. Doped Ag_2O/Sb_2O_3 NPs display improved performance due to the large-active surface area, which increases the conductivity and current responses of the Ag_2O/Sb_2O_3 NPs/Nafion/GCE assembly during electrochemical investigations.

Structural analyses

To assess the photosensitivity of the prepared Ag_2O/Sb_2O_3 NPs, UV/vis spectroscopy analysis was carried out. Absorption spectrum of the Ag_2O/Sb_2O_3 NPs was measured as a function of wavelength as presented in Fig. 1(a). The observed spectrum shows an intense and wide absorption band at 307 nm identical to the transition of valence band electron of Ag_2O/Sb_2O_3 NPs from lower to higher energy level.[14,22] According to eqn (vi), the calculated band gap energy is 4.04 eV.[23]

$$E_{bg} = 1240/\lambda_{max} \quad \text{(vi)}$$

The synthesized Ag_2O/Sb_2O_3 NPs were subjected to FTIR investigation to determine the functional properties of the atom or molecule from the corresponding atomic and molecular vibrations. FTIR was performed in the range of 450–4000 cm^{-1} as illustrated in Fig. 1(b). From the observed FTIR spectrum, the peaks were obtained at 551 and 772 cm^{-1}. The existence of major peaks at 551 and 772 cm^{-1} resulted from the stretching vibration of metallic (Ag–O & Sb–O) oxygen bonds respectively.[22,24] To investigate the structural properties and phase (crystallinity) of the synthesized Ag_2O/Sb_2O_3 NPs, XRD was implemented. The resultant XRD pattern illustrated in Fig. 1(c) conveys that the synthesized Ag_2O/Sb_2O_3 NPs consist of distinct phases for Ag_2O and Sb_2O_3. According to the XRD diffraction pattern, the reflected peaks of Ag_2O denoted as θ are (111), (200), (220), (222) and (311), which are analogous with previous reports on bulk Ag_2O[25–27] and JCPDS card no. 4-0783. In addition, the several peaks of Sb_2O_3 indicated as β represent the phases (012), (110), (210), (410), (503), and (602) and matched well with those reported in the literature.[28,29] The crystal size of the nanomaterial can be measured from its XRD diffraction pattern by implementation of the Scherrer equation, which is presented in eqn (vii).

$$D = 0.9\lambda/\beta \cos\theta \quad \text{(vii)}$$

Here, λ is the wavelength (X-ray radiation = 1.5418 Å) and β is the full width at half maximum, corresponding to highest intense peak, and θ is the diffraction angle.[30] The average calculated cross sectional diameter of Ag_2O/Sb_2O_3 NPs is 21.38 nm.

Morphological and elemental analyses

FESEM imaging was performed to study the morphology of the synthesized Ag_2O doped Sb_2O_3 NPs and the resultant representative low and high magnification images of FESEM are

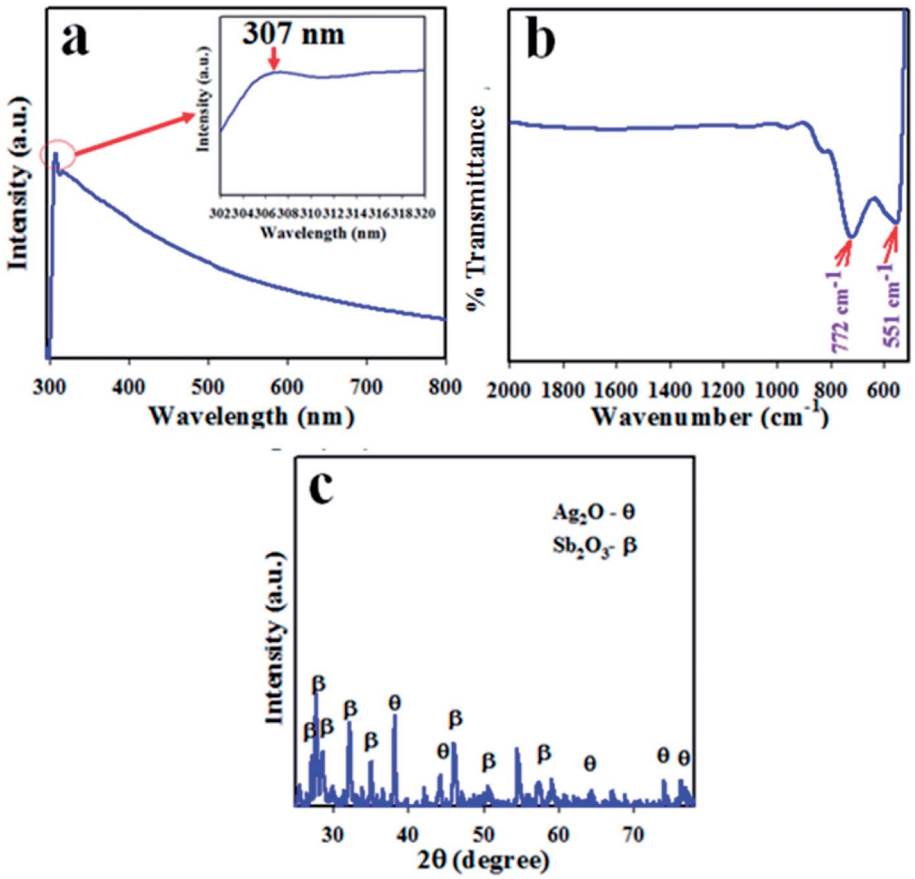

Fig. 1 Optical and morphological evaluation by (a) UV spectrum, (b) FTIR and (c) XRD pattern of the Ag_2O/Sb_2O_3 nanoparticles.

presented in Fig. 2(a and b). The average diameter of the doped Ag_2O/Sb_2O_3 NPs is calculated as 35.3 nm, in the range of 30.0 to 40.0 nm. From FESEM investigation, it is confirmed that the produced nano-doped materials have the shape of nanoparticles.[31–33] The FESEM investigation has similarities with the argument of EDS analysis illustrated in Fig. 2(c and d) and the

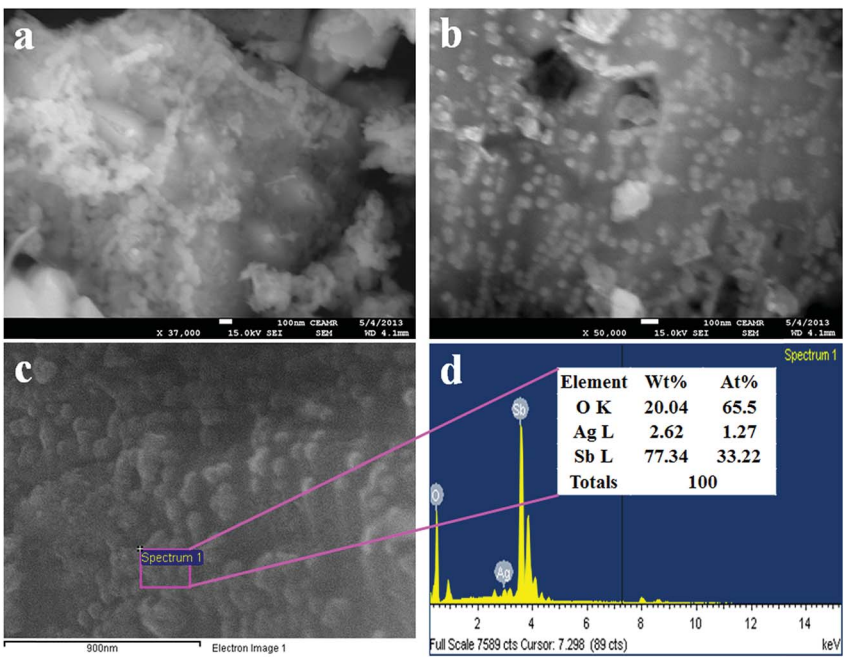

Fig. 2 (a and b) FESEM images from low to high magnification and (c and d) elemental analysis of the Ag_2O/Sb_2O_3 NPs.

structural composition of prepared nanoparticles are authenticated from the EDS investigation. Therefore, the EDS analysis reveals that silver (Ag), oxygen (O), and antimony (Sb) exist in the NPs in the composition O (20.04 wt%), Sb (77.34 wt%), and Ag (2.62 wt%). No other supplementary peaks were detected and the confirmation about the existence of O, Sn and Cd in the prepared nanomaterials is accredited by EDS analysis.[14,34]

Binding energy analysis

The quantitative spectroscopic technique of XPS was applied to investigate the nature of species existing in the prepared Ag_2O/Sb_2O_3 NPs. Generally, the atomic composition with corresponding chemical formula and the oxidation state of the species present in the nanomaterial can be scrutinized efficiently using this technique.[35] The XPS spectra of the Ag_2O/Sb_2O_3 NPs is shown in Fig. 3. Two main identical peaks of Ag3d orbit of the synthesized Ag_2O/Sb_2O_3 NPs can be observed, as illustrated in Fig. 3(a). Apparently, these two peaks are equal and indicate equal oxidation states of Ag. The observed binding energies of $Ag3d_{5/2}$ and $Ag3d_{3/2}$ are 368 and 373 eV, respectively, which are the characteristic values of the oxidation of Ag^+ in Ag_2O.[36,37] The O1s peak of the Ag_2O/Sb_2O_3 NPs could be clearly recognized and is centered at 533 eV as represented in Fig. 3(b). It can be ascribed to the Ag–O bond of Ag_2O.[38] The XPS spectrum of Sb3d is shown in Fig. 3(c) and two characteristic peaks of $Sb3d_{5/2}$–O1s and $Sb3d_{3/2}$ are identified centered at 533 eV and 540 eV, respectively. The peaks significantly confirmed the attribution of Sb^{3+} state.[39,40]

Applications: detection of 3-methoxyphenol by Ag_2O/Sb_2O_3 NPs

The electrochemical sensor based on Ag_2O/Sb_2O_3 NPs/Nafion/GCE was constructed with the aim to detect the selective toxin (3-methoxyphenol) in phosphate buffer system. The projected chemical sensor has several benefits including high stability in air, inert nature in chemical environment, enhanced electrochemical activity during detection, easy in terms of handling, assembly and fabrication, and above all, safe chemo-characteristics. To prepare the chemical sensor selective to 3-methoxyphenol, a slurry of Ag_2O/Sb_2O_3 NPs was prepared in ethanol, deposited as a uniform thin layer onto the GCE (commercial glassy carbon electrode) and the modified GCE was dried at ambient conditions. To improve the binding strength between the uniform layer of NPs and the GCE, a drop of Nafion (5% Nafion suspension in ethanol) was added and the electrode was placed inside an oven at 35.0 °C temperature until the conducting film was dried completely. Nafion improves the binding strength as well as the electron transfer rate of the modified GCE.[41,42] During the sensing performance of 3-methoxyphenol electrochemical sensor in the desired phosphate buffer system, the current *vs.* potential of thin-film Ag_2O/Sb_2O_3 NPs/binder/GCE electrochemical sensor was assessed. The holding period of the electrometer was set at 1.0 s. The proposed detection (oxidation) mechanism of 3-methoxyphenol is illustrated in Scheme 2. As stated in the proposed oxidation mechanism of 3-methoxyphenol, an enrichment of electron in the buffer medium is observed, which causes the amendment of

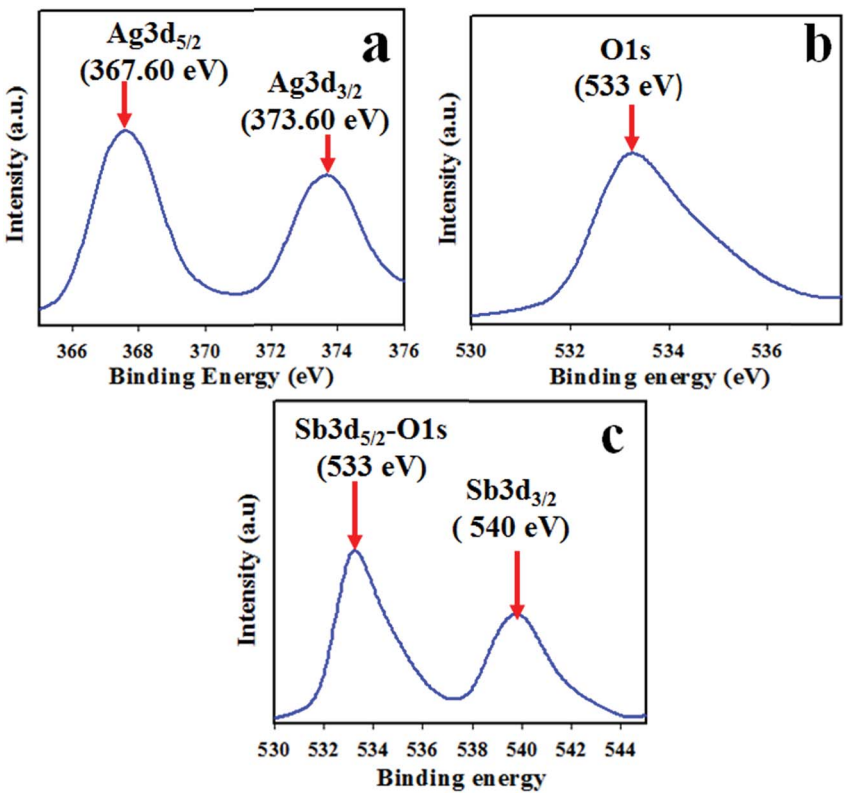

Fig. 3 Binding energy analysis of Ag_2O/Sb_2O_3 NPs by XPS. (a) Spin orbit Ag3d level, (b) O1s, and (c) spin orbit Sb3d level.

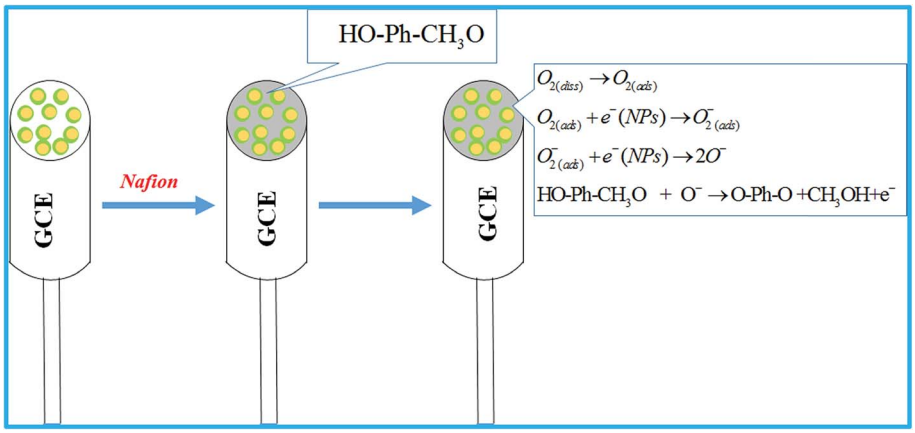

Scheme 2 The expected mechanism for determination of 3-methoxyphenol by Ag_2O/Sb_2O_3 nanoparticles using electrochemical approach.

I–V response. At the beginning of 3-methoxyphenol oxidation, dissolved oxygen is absorbed on the surface of the working electrode and ionized into O^- ion, which reacts with 3-methoxyphenol to form *p*-benzoquinone, methanol and electron as presented in reactions (viii) to (xi). Oxidation of 3-methoxyphenol is similar to other reported articles.[15,43] A pictorial representation of the application of the Ag_2O/Sb_2O_3 NPs modified electrode is demonstrated in Scheme 2.

According to the electrochemical oxidation process of 3-methoxyphenol, an electron is released from the conduction band and is responsible for the amendment of *I–V* response of the Ag_2O/Sb_2O_3 NPs/binder/GCE electrochemical sensor.

$$O_{2(diss)} \rightarrow O_{2(ads)} \quad \text{(viii)}$$

$$O_{2(ads)} + e^-(NPs) \rightarrow O_{2(ads)}{}^- \quad \text{(ix)}$$

$$O_{2(ads)}{}^- + e^-(NPs) \rightarrow 2O^- \quad \text{(x)}$$

$$HO\text{–}Ph\text{–}CH_3O + O\text{–} \rightarrow O\text{–}Ph\text{–}O + CH_3OH + e^- \quad \text{(xi)}$$

The assembled Ag_2O/Sb_2O_3 NPs/binder/GCE electrode is not equally responsive in all buffer media. Therefore, the fabricated electrode was investigated in various phosphate buffer systems (pH of 5.7, 6.5, 7.0, 7.5 and 8.0) to obtain the highest *I–V* response. As observed from Fig. 4(a), the projected electrochemical sensor is found to give a maximum response in pH 6.5 at an applied potential of 0 to +1.5 V.

To investigate the selectivity of the assembled chemical sensor, a number of toxins such as acetone, 2-nitrophenol, 3-methoxyphenol, 4-aminophenol, 4-methoxyphenol, bisphenol A, methanol, ammonium hydroxide, and *p*-nitrophenol were examined at micro-level concentrations and an applied potential of 0 to +1.5 V in phosphate buffer medium of pH 6.5; the resultant *I–V* responses are illustrated in Fig. 4(b). As perceived from Fig. 4(b), 3-methoxyphenol exhibited the highest current response among all toxins. As reproducibility is a very important factor in the analytical performance of an electrochemical sensor, the 3-methoxyphenol sensor was assessed at a 0.9 μM concentration of 3-methoxyphenol and an applied potential 0 to +1.5 V in pH 6.5 phosphate buffer medium as demonstrated in Fig. 4(c). The five runs were practically indistinguishable and provides information about the reliability of detection of toxin in real-time in the field. To verify the accuracy of reproducibility in performance, the relative standard deviation (RSD) of current data at applied potential +1.2 V was measured and it was found to be 1.33%. Thus, it can be predicted that the proposed electrochemical sensor based on Ag_2O/Sb_2O_3 NPs/binder/GCE is proficient enough to detect 3-methoxyphenol in real environmental samples. The response time is yet another analytical performance parameter to measure the efficiency of the electrochemical sensor. This test was performed using 0.9 μM concentration of 3-methoxyphenol solution. The excellent result for the response time of 12.0 second is obtained as illustrated in Fig. 4(d). This result might be satisfactory.

The intensity of *I–V* response of 3-methoxyphenol chemical sensor varies with the concentration of 3-methoxyphenol. Therefore, the *I–V* responses of Ag_2O/Sb_2O_3 NPs/binder/GCE sensor were measured at various concentrations of 3-methoxyphenol ranging from 0.9 mM to 0.09 nM as shown in Fig. 5(a). This was experimented at an applied potential of 0 to +1.5 V in phosphate buffer medium of pH 6.5. As demonstrated in Fig. 5(a), *I–V* responses are distinguishable from lower to higher concentrations. Therefore, it can be concluded that *I–V* responses are amplified with increasing concentration of the electrolyte (3-methoxyphenol). To scale up the analytical limit of the proposed 3-methoxyphenol electrochemical sensor, a linear calibration curve was plotted at an applied potential of +1.2 V from the lower-higher concentration of 3-methoxyphenol solution as shown in Fig. 5(b). The regression coefficient (r^2: 0.99), sensitivity (11.67 μA μM^{-1} cm^{-2}), linear dynamic ranges (LDR: 0.09 nM to 0.09 mM) and the detection limit (LD: 0.08 ± 0.004 nM) were calculated from the resultant calibration curve at signal to noise ratio of 3. The estimated analytical performances including sensitivity, linear dynamic range (LDR) and detection limit (DL) are appreciable.

As seen from Fig. 5(a), *I–V* responses varied with the corresponding concentration of 3-methoxyphenol. A similar tendency for current *vs.* potential has been reported by previous

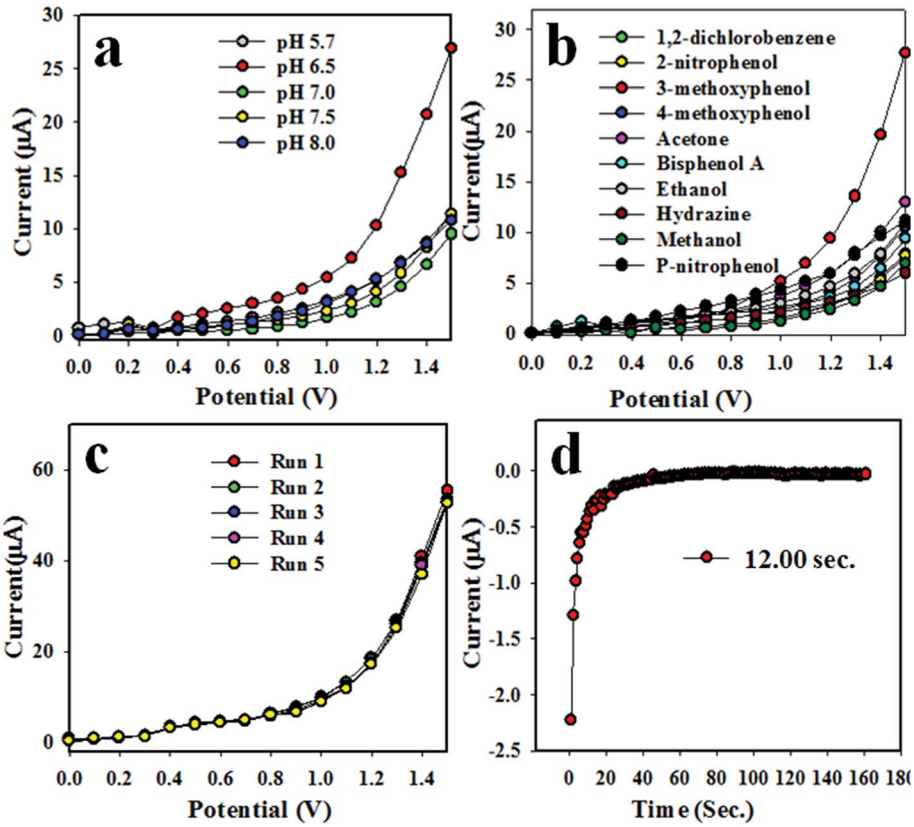

Fig. 4 Optimization of the 3-methoxyphenol sensor with Ag_2O/Sb_2O_3 NPs. (a) pH optimization, (b) selectivity, (c) repeatability, and (d) response time.

authors.[15,44,45] At the beginning of 3-methoxyphenol detection performance, the targeted 3-methoxyphenol molecules occupy a small fraction of surface on Ag_2O/Sb_2O_3 NPs/binder/GCE film and the corresponding oxidation reaction of the 3-methoxyphenol starts progressively. With increasing analyte (3-methoxyphenol) concentration in the buffer medium, the reaction on the working electrode surface is increased and a larger surface coverage corresponding to the 3-methoxyphenol molecules is observed. On additional enrichment of the analyte (3-methoxyphenol) concentration, a highly moderate current *versus* potential response is experimented and the surface coverage by the corresponding analyte on the surface of Ag_2O/Sb_2O_3 NPs/GCE working electrode is maximum. On further enrichment of analyte concentration, the surface coverage by 3-methoxyphenol molecules touches its saturation. As we observed, the proposed 3-methoxyphenol sensor is shows a very short response time of around 12 s, which is required for the steady state saturation. Therefore, it can be summarized that

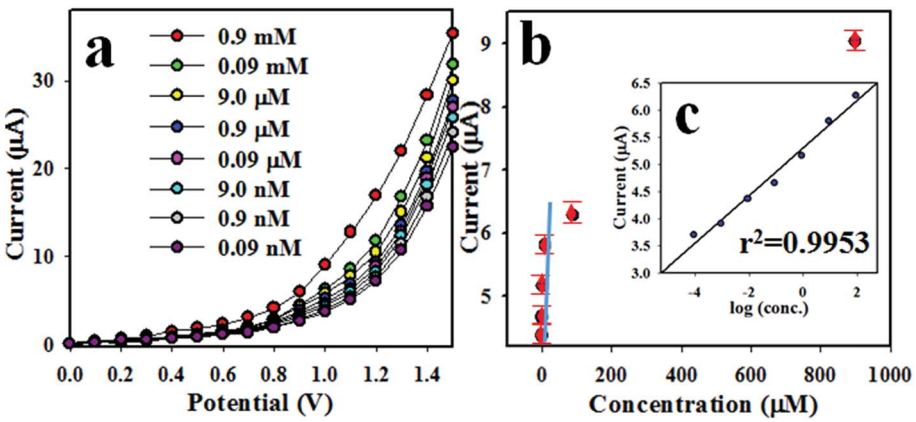

Fig. 5 (a) Concentration variation of 3-methoxyphenol sensor based on Ag_2O/Sb_2O_3 NPs/GCE by *I*–*V* method and (b) calibration curve (inset: log[3-methoxyphenol. conc.] *vs.* current).

Table 1 Performance of 3-methoxyphenol and other phenolic sensors with various nanomaterials or nanocomposites by electrochemical approaches[a]

Modified electrode	DL	LDR	Sensitivity	Ref.
NiS_2-CNT NCs/GCE	30 pM	0.01 nM–10.0 mM	0.63 μA μM^{-1} cm^{-2}	15
3D graphene micropiller/GCE	50 nM	50.0 nM–2.0 μM	3.9×10^{-3} μA μM^{-1} cm^{-2}	16
Ag-MWCNT/GCE	0.36 nM	0.4 nM–40.0 mM	3.829×10^{-3} μA μM^{-1} cm^{-2}	17
MWCNT/GCE	90 nM	0.2–1.6 μM	7.0 μA μM^{-1} cm^{-2}	44
NPG thin-film/GCE	0.5 μM	0.5–200 μM	0.15 μA μM^{-1} cm^{-2}	45
Ag_2O/Sb_2O_3 NPs/GCE	0.08 nM	0.09 nM–0.09 mM	11.67 μA μM^{-1} cm^{-2}	This study

[a] DL (detection limit), LDR (linear dynamic range).

Table 2 Measured concentration of 3-methoxyphenol analytes in real sample[a]

	Observed current (μA)						
Real sample	R1	R2	R3	R4	Average (μA)	Calculated conc. (μM)	% RSD
Industrial effluents	1.56	1.67	1.69	1.77	1.6725	0.160853	5.18
PC baby bottle	0.509	0.512	0.457	0.468	0.4865	0.046789	5.78
Drinking-water-battle	0.460	0.475	0.478	0.476	0.4723	0.045423	1.75
PVC food packaging	0.860	0.879	0.853	0.733	0.8313	0.079950	7.99

[a] R (reading), RSD (relative standard deviation).

the proposed 3-methoxyphenol chemical sensor based on Ag_2O/Sb_2O_3 NPs/GCE assembly can be engaged for successful detection of the targeted toxin (3-methoxyphenol). As perceived from Fig. 5(b), the current data are constantly distributed along the linear plot in the concentration range of 0.09 nM–0.09 mM, which is characterized as the LDR and this exploration is considered as the reliability of the method. Since, the 3-methoxyphenol chemical sensor exhibited a moderately high sensitivity of 11.67 μA μM^{-1} cm^{-2}, it can be considered to have super adsorption capacity, active catalytic decomposition ability, and excellent biocompatibility.[15,17,45] In terms of selectivity and detection limit, the proposed 3-methoxyphenol chemical sensor based on Ag_2O/Sb_2O_3 NPs has showed a reasonably good performance compared to other electrochemical sensors tested earlier as illustrated in Table 1. To measure the electrochemical activities of individual (Ag_2O NPs and Sb_2O_3 NPS) and combinational (Ag_2O/Sb_2O_3 NPs) metal oxides, a number of experiments were conducted at an applied potential of 0 to +1.5 V and 0.9 μM concentration of 3-methoxyphenol in phosphate buffer medium of pH 6.5 as demonstrated in Fig. S1 in the ESI.† It is observed that the combinational effect of Ag_2O/Sb_2O_3 NPs showed a supreme *I–V* response. Therefore, it can be mentioned that the fabricated 3-methoxyphenol chemical sensor is simple and efficient in detecting 3-methoxyphenol by the current *versus* potential method in an electro-chemical approach. The sensing performance of the earlier testified metal oxides based phenolic sensors are associated and summarized in Table 1.[15–17,46]

The analysis of real samples

To validate the probe, the 3-methoxyphenol sensor based on Ag_2O/Sb_2O_3 NPs coated onto GCE with conducting binder was used to detect 3-methoxyphenol in various real and extracted environmental samples. We measured 3-methoxyphenol in industrial effluents, PC baby bottle, PC water bottle, and PVC food packaging bag. The results showed that 3-methoxyphenol detection is possible from the environmental samples, which are represented in Table 2.

Conclusions

In summary, doped Ag_2O/Sb_2O_3 nanoparticles were prepared by a facile hydrothermal process and characterized by SEM, EDS, FTIR, XPS and XRD. A thin layer of Ag_2O/Sb_2O_3 NPs was applied onto a GCE using a conducting binder to prepare sensor probe for 3-methoxyphenol detection. The proposed 3-methoxyphenol chemical sensor has been shown to have excellent performance based on the electrochemical parameters such as detection limit, linear dynamic range, sensitivity, repeatability, robustness, stability, and response time. The calibration plot is linear over a large concentration range. The calculated selectivity and detection limit is 11.67 μA μM^{-1} cm^{-2} and 0.08 pM, respectively, at signal to noise ratio of 3. Therefore, this sensor can be used for the detection of the toxic chemical existing in real environmental effluents to ensure ecological and environmental safety.

Conflicts of interest

There are no conflicts to declare.

Acknowledgements

Center of Excellence for Advanced Materials Research (CEAMR) at King Abdulaziz University, Jeddah, Saudi Arabia is highly

acknowledged for providing their lab facilities for the fabrication, characterization, and application of the sensors.

References

1 I. G. Vincent, G. Angeletti and A. Bjorseth, *Organic Micropollutants in the Aquatic Environment*, Kluwer Academic Publishers, Dordrecht, 1991.
2 J. Li, D. Kuang, Y. Feng, F. Zhang, Z. Xu and M. Liu, A graphene oxide-based electrochemical sensor for sensitive determination of 4-nitrophenol, *J. Hazard. Mater.*, 2012, **201**, 250–259.
3 P. Deng, Z. Xu, Y. Feng and J. Li, Electrocatalytic reduction and determination of *p*-nitrophenol on acetylene black paste electrode coated with salicylaldehyde modified chitosan, *Sens. Actuators, B*, 2012, **168**, 381–389.
4 R. M. A. Tehrani, H. Ghadimi and S. A. Ghani, Electrochemical studies of two diphenols isomers at graphene nanosheet-poly (4-vinyl pyridine) composite modified electrode, *Sens. Actuators, B*, 2013, **177**, 612–619.
5 F. Karim and A. N. M. Fakhruddin, Recent advances in the development of biosensor for phenol: a review, *Sci. Biotechnol.*, 2012, **11**, 261–274.
6 R. W. Takashima and K. Kaneto, Amperometric Phenol biosensor based pyrrole-copolymer film, *Sens. Actuators, B*, 2004, **102**, 271–277.
7 A. Arecchi, M. Scampicchio, S. Drusch and S. Mannino, Nanofibrous membrane based tyrosinase-biosensor for the detection of phenolic compounds, *Anal. Chim. Acta*, 2010, **659**, 133–136.
8 C. D. Chriswell, R. C. Chang and J. S. Fritz, Chromatographic determination of phenols in water, *Anal. Chem.*, 1975, **47**, 1325–1329.
9 J. Poerschmann, Z. Zhang, F. D. Kopinke and T. Pawliszyn, Solid phase microextraction for determining the distribution of chemicals in aqueous matrices, *Anal. Chem.*, 1997, **69**, 597–600.
10 C. Nistor, J. Emnéus, L. Gorton and A. Ciucu, Improved stability and altered selectivity of tyrosinase based graphite electrodes for detection of phenolic compounds, *Anal. Chim. Acta*, 1999, **387**, 309–326.
11 D. A. Oriero, I. O. Gyan, B. W. Bolshaw, I. F. Cheng and D. E. Aston, Electrospun biocatalytic hybrid silica–PVA-tyrosinase fiber mats for electrochemical detection of phenols, *Microchem. J.*, 2015, **118**, 166–175.
12 A. Umar, M. S. Akhtar, G. N. Dar and S. Baskoutas, Low-temperature synthesis of α-Fe_2O_3 hexagonal nanoparticles for environmental remediation and smart sensor applications, *Talanta*, 2013, **116**, 1060–1066.
13 M. M. Rahman, S. B. Khan, H. M. Marwani and A. M. Asiri, $ASnO_2$–Sb_2O_3 nanocomposite for selective adsorption of lead ions from water samples prior to their determination by ICP-OES, *Microchim. Acta*, 2015, **182**, 579–588.
14 M. M. Rahman, S. B. Khan, A. Jamal, M. Faisal and A. M. Asiri, Fabrication of highly sensitive acetone sensor based on sonochemically prepared as-grown Ag_2O nanostructures, *Chem. Eng. J.*, 2012, **192**, 122–128.
15 M. M. Rahman, J. Ahmed, A. M. Asiri, I. A. Siddiquey and M. A. Hasnat, Development of 4-methoxyphenol chemical sensor based on NiS_2 -CNT nanocomposites, *J. Taiwan Inst. Chem. Eng.*, 2016, **64**, 157–165.
16 F. Liu, Y. Piao, J. S. Choi and T. S. Seo, Three-dimensional graphene micropillar based electrochemical sensor for phenol detection, *Biosens. Bioelectron.*, 2013, **50**, 387–392.
17 M. M. Rahman, A. Khan and A. M. Asiri, Chemical sensor development based on poly(oanisidine) silverized–MWCNT nanocomposites deposited on glassy carbon electrodes for environmental remediation, *RSC Adv.*, 2015, **5**, 71370–71378.
18 M. M. Rahman, S. B. Khan, H. M. Marwani and A. M. Asiri, A SnO_2–Sb_2O_3nanocomposite for selective adsorption of lead ions from water samples prior to their determination by ICP-OES, *Microchim. Acta*, 2015, **182**, 579–588.
19 M. M. Rahman, S. B. Khan, A. Jamal, M. Faisal and A. M. Asiri, Fabrication of highly sensitive acetone sensor based on sonochemically prepared as-grown Ag_2O nanostructures, *Chem. Eng. J.*, 2012, **192**, 122–128.
20 M. M. Rahman, S. B. Khan, A. M. Asiria and A. G. Al-Sehemi, Chemical sensor development based on polycrystalline gold electrode embedded low-dimensional Ag_2O nanoparticles, *Electrochim. Acta*, 2013, **112**, 422–430.
21 M. M. Rahman, S. B. Khan, H. M. Marwani and A. M. Asiri, Selective Divalent Cobalt Ions Detection Using Ag_2O_3–ZnO Nanocones by ICP-OES Method for Environmental Remediation, *PLoS One*, 2014, **9**, 114084.
22 K. R. Nemadea and S. A. Waghuley, LPG sensing performance of CuO–Ag_2O bimetallicoxide nanoparticles, *St. Petersburg Polytechnical University Journal: Physics and Mathematics*, 2015, **1**, 249–255.
23 M. M. Rahmana, S. B. Khana, A. M. Asiri and A. G. Al-Sehemi, Chemical sensor development based on polycrystalline gold electrode embedded low-dimensional Ag_2O nanoparticles, *Electrochim. Acta*, 2013, **112**, 422–430.
24 F. Chen, Q. Yang, C. Niu, X. Li, C. Zhang and G. Zeng, Plasmonic photocatalyst Ag@AgCl/$ZnSn(OH)_6$: synthesis, characterization and enhanced visiblelight photocatalytic activity in the decomposition of dyes and phenol, *RSC Adv.*, 2015, **5**, 63152–63164.
25 P. K. Khanna, N. Singh, S. Charan, V. V. V. S. Subbarao, R. Gokhale and U. P. Mulik, Synthesis and characterization of Ag/PVA nanocomposite by chemical reduction method, *Mater. Chem. Phys.*, 2005, **93**, 117–121.
26 P. K. Khanna, N. Singh, S. Charan and A. K. Viswanath, Synthesis of Ag/polyaniline nanocomposite *via* an *in situ* photo-redox mechanism, *Mater. Chem. Phys.*, 2005, **92**, 214–219.
27 M. A. S. Sadjadi, B. Sadeghi, M. Meskinfam, K. Zare and J. Azizian, Synthesis and characterization of Ag/PVA nanorods by chemical reduction method, *Phys. E*, 2008, **40**, 3183–3186.
28 M. O. G. Perez, J. L. G. Fierro and M. A. Banares, Tunning the Nb addition to Sb–V–O catalysts for an efficient promotion of the ammoxidation of propane to acrylonitrile, *Catal. Today*, 2006, **118**, 366–372.

29 S. A. Mahapure, P. K. Palei, L. K. Nikam, R. P. Panmand, J. D. Ambekar, S. K. Apte and B. B. Kale, Novel nanocrystalline zinc silver antimonite ($ZnAg_3SbO_4$): an efficient & ecofriendly visible light photocatalyst with enhanced hydrogen generation, *J. Mater. Chem. A*, 2013, **1**, 12835–12840.

30 R. Jenkins and R. L. Snyder, *X-ray Powder Diffractometry. An Introduction*, John Wiley & Sons, 1994, vol. 138, pp. 750–950.

31 B. Nithyaja, H. Misha and V. P. N. Nampoori, Synthesis of Silver Nanoparticles in DNA Template and Its Influence on Nonlinear Optical Properties, *Nanosci. Nanotechnol.*, 2012, **2**, 99–103.

32 N. Krithiga, A. Rajalakshmi and A. Jayachitra, Green Synthesis of Silver Nanoparticles Using Leaf Extracts of Clitoria ternatea and Solanum nigrum and Study of Its Antibacterial Effect against Common Nosocomial Pathogens, *J. Nanosci.*, 2015, 1–8.

33 G. Geoprincy, P. Saravanan, N. N. Gandhi and S. Renganathan, A nobel approach for studying the combined antimicrobial effects of silver nanoparticles and antibiotics through agar over layer method and disk diffusion, *Dig. J. Nanomater. Biostruct.*, 2011, **6**, 1557–1565.

34 J. Baharara, F. Namvar, T. Ramezani, N. Hosseini and R. Mohamad, Green Synthesis of Silver Nanoparticles using Achillea biebersteinii Flower Extract and Its Anti-Angiogenic Properties in the Rat Aortic Ring Model, *Molecules*, 2014, **19**, 4624–4634.

35 S. S. Patil, M. G. Mali, M. S. Tamboli, D. R. Patil, M. V. Kulkarni, H. Yoon, H. Kim, S. S. Al-Deyab, S. S. Yoonc, S. S. Kolekarb and B. B. Kale, Green approach for hierarchical nanostructured Ag–ZnO and their photocatalytic performance under sunlight, *Catal. Today*, 2016, **260**, 126–134.

36 W. Fan, S. Jewell, Y. She and M. K. H. Leung, In situ deposition of Ag–Ag_2S hybrid nanoparticles onto TiO_2 nanotube arrays towards fabrication of photoelectrodes with high visible light photoelectrochemical properties, *Phys. Chem. Chem. Phys.*, 2014, **16**, 676–680.

37 Z. Chen, W. Wang, Z. Zhang and X. Fang, High-Efficiency Visible-Light-Driven Ag_3PO_4/AgI Photocatalysts: Z-Scheme Photocatalytic Mechanism for Their Enhanced Photocatalytic Activity, *J. Phys. Chem. C*, 2013, **117**, 19346–19352.

38 F. H. Cincotto, T. C. Canevari, A. M. Campos, R. Landers and S. A. S. Machado, Simultaneous determination of epinephrine and dopamine by electrochemical reduction on the hybrid material SiO_2/graphene oxide decorated with Ag nanoparticles, *Analyst*, 2014, **139**, 4634–4640.

39 J. K. Liang, H. L. Su, C. L. Kuo, S. P. Kao, J. W. Cuia, Y. C. Wua and J. C. A. Huang, Structural, Optical and Electrical Properties of Electrodeposited Sb-Doped ZnO Nanorod Arrays, *Electrochim. Acta*, 2014, **125**, 124–132.

40 M. Ahmad, C. Pan and J. Zhu, Electrochemical determination of L-Cysteine by an elbow shaped, Sb-doped ZnO nanowire-modified electrode, *J. Mater. Chem.*, 2010, **20**, 7169–7174.

41 S. Ren, C. Li, X. Zhao, Z. Wu, S. Wang, G. Sun, Q. Xin and X. Yang, Surface modification of sulfonated poly(ether ether ketone) membranes using nafion solution for direct methanol fuel cells, *J. Membr. Sci.*, 2005, **247**, 59–63.

42 Z. Wang, G. Liu, L. Zhang and H. Wang, Electrochemical detection of trace cadmium in soil using a Nafion/stannum film-modified molecular wire carbon paste electrodes, *Ionics*, 2013, **19**, 1687–1693.

43 H. B. Balkhoyor, M. M. Rahman and A. M. Asiri, Effect of Ce doping into ZnO nanostructures to enhance the phenolic sensor performance, *RSC Adv.*, 2016, **6**, 58236.

44 M. M. Rahman, H. B. Balkhoyor and A. M. Asiri, Phenolic sensor development based on chromium oxide-decorated carbon nanotubes for environmental safety, *J. Environ. Manage.*, 2017, **188**, 228–237.

45 S. Korkut, M. S. Kilic and E. Erhan, Modified poly(pyrrole) film based biosensors for phenol detection, *Int. J. Chem. Mol. Nucl. Mater. Metall. Eng.*, 2015, **9**, 439–442.

46 G. Scandurra, A. Antonella, C. Ciofi, G. Saitta and M. Lanza, Electrochemical detection of *p*-aminophenol by flexible devices based on multi-wall carbon nanotubes dispersed in electrochemically modified nafion, *Sensors*, 2014, **14**, 8926–8939.